International Journal of Research in Engineering and Applied Sciences(IJREAS)
Available online at http://euroasiapub.org
Vol. 8 Issue 6, June-2018,
ISSN (O): 2249-3905, ISSN(P): 2349-6525 | Impact Factor: 7.196 |

DESIGN OF A NOVEL POWER ELECTRONICS ARCHITECTURE FOR HIGH VOLTAGE ELECTRIC HYBRID VEHICLES

Dr. Puneet Kaur
Assistant Professor (Electrical and Electronics Engg)
UIET, Panjab University, Chandigarh, India.
Email: puneetee@pu.ac.in

ABSTRACT

The development of innovative power electronics architectures and systems is being spurred forward because of the ongoing search for electric hybrid vehicles (EHVs) of the next generation. The primary objective of this paper is to concentrate on enhancing the integration, performance, and efficiency of components that can be used in EHV power electronics. These innovative designs, such as series, parallel or series/parallel, complex battery management systems (BMS), and integrated thermal management solutions, are being investigated and presented in order to address the issues of power density, heat dissipation, and reliability. By conducting thorough simulation studies, the purpose of this paper is to shed light on the design, implementation, and performance evaluation of novel power electronics architectures for next-generation electric high-voltage vehicles (EHVs).

Keywords: electric hybrid vehicles, power electronics, renewable energy integration

1.INTRODUCTION

As a result of the urgent requirement to reduce our dependency on fossil fuels and the pollution that they generate, the automobile industry has undergone a paradigm shift toward forms of transportation that are less harmful to the environment. Within the context of this paradigm, electric hybrid vehicles, also known as EHVs, have emerged as a potential link between cars that are powered solely by electric propulsion and those that are powered by conventional internal combustion engines. As a result of the integration of electric and internal combustion engine technology, electric hybrid vehicles (EHVs) provide numerous advantages over conventional automobiles. These advantages include improvements in fuel economy, reduced emissions of pollutants, and increased driving range [1-2].

To extend the possibilities of electric high-voltage vehicles, new power electronics architectures and technologies are essential. There are a great number of components in a vehicle that are dependent on power electronics in order to convert and manage electrical energy. Some examples of these components include batteries, motors, and internal combustion engines. The performance of the vehicle, its dependability, and the user experience can all be maximized through the implementation of power electronics systems that are efficient and also optimize energy consumption.

In electric hybrid vehicles (EHVs), power electronics encompass a wide variety of systems and technologies that contribute to the control and efficiency of electrical energy. Every component of the car is necessary for its functioning and efficiency; converters, inverters, controllers, and battery management systems (BMS) are not an exception to this rule.

When it comes to the construction of next-generation electric hybrid vehicles, one of the primary objectives is to enhance the efficiency of power conversion [3-4]. Advanced converter topologies, such as resonant converters and multi-level converters, are examples of converter topologies that exceed more standard systems in terms of efficiency and power quality [5-7].

The enhancement of energy storage capacity is yet another very essential subject that should be focused on. Efficiency in battery management systems is essential for ensuring that charging and discharging rates are suitable, that battery life is extended, and that performance is monitored. New battery management system (BMS) advancements include cell balancing approaches, thermal management tactics, and new algorithms for state-of-charge (SoC) estimations. These innovations are designed to maintain the health and dependability of batteries in a variety of operating conditions.

Moreover, the incorporation of renewable energy sources such as solar panels or regenerative braking systems presents opportunities to increase the charging capacity of automobiles and reduce reliance on the power grid. In order to achieve the highest possible level of efficiency in terms of energy collection and utilization, power electronics systems make it possible to seamlessly incorporate a variety of renewable sources into the power architecture of the vehicle.

The control of thermal energy is also taken into consideration in the design of innovative power electronics for EHVs[8-10]. The effective dissipation of heat is of utmost importance for the performance and durability of components, particularly in high-power applications such as electric propulsion systems. The use of heat exchangers and liquid cooling systems are two examples of integrated thermal management technologies that contribute to the regulation of temperatures and the general enhancement of system efficiency.

Not only do we require technical advancements, but we also require rules and regulations that are specifically designed for these systems in order to achieve our goal of making EHV power electronics safe, interoperable, and dependable across all platforms[11-13]. Manufacturers are required to comply with these regulations in order to ensure that they earn the trust of consumers and meet the high expectations that consumers have about quality and performance.

In this paper optimized design of the parallel and the series/parallel architectures for developing HEV has been discussed.

International Journal of Research in Engineering and Applied Sciences(IJREAS)
Available online at http://euroasiapub.org
Vol. 8 Issue 6, June-2018,
ISSN (O): 2249-3905, ISSN(P): 2349-6525 | Impact Factor: 7.196 |

2.VEHICLE MODELLING AND ROAD MISSIONS

Series hybrid vehicles are the main subject of this evaluation. Nevertheless, considering both series and parallel architectures is also a consideration, as a comparison between the two is demonstrated.

2.1 Resistance Force Modelling

One may calculate the losses as a function of steady-state working points since the component dynamics is insignificant to the energetic evaluations of the system. Equation (1) derives the resisting force on the vehicle, while Equations (2), (3), and (4) display the force equations. As a result, the suggested vehicle model is quasi-stationary [14].

$$F_{RESISTANT} = F_{slope} + F_{rolling} + F_{aerodynamics} \quad (1)$$

$$F_{slope} = mg\sin(\alpha) \quad (2)$$

$$F_{rolling} = mgC_r\cos(\alpha) \quad (3)$$

$$F_{aerodynamics} = \frac{1}{2}\rho C_X S v^2 \quad (4)$$

where g is the universal gravitational constant [m/s^2], m represents the vehicle mass is the air density ρ[°] is the road inclination, Cr is the rolling coefficient, α[kg], [kg/m3], and v is the vehicle speed [m/s]. C_x is the aerodynamic coefficient, and S is the front section of the vehicle [m^2]. Starting from Equation (1), the torque which results is obtained as in Equation (5):

$$T_{RESISTANT} = \frac{F_{RESISTANT} R_{wheel}}{\tau} \quad (5)$$

The wheel radius (R_{wheel}) and transmission ratio (T_{wheel}) are used to denote these parameters, respectively. Using the differential equation (6), we can determine the vehicle's speed:

$$T_{motor} - T_{RESISTANT} = J\frac{d\omega}{dt} \quad (6)$$

where:

$$\omega = \frac{2\pi\tau}{R_{wheel}} \quad (7)$$

$$J = \frac{mR_{wheel}^2}{\tau^2} + J_{motor} \quad (8)$$

where T_{motor} [Nm] denotes the machine's torque, which is negative when engaging in regenerative braking, Motor J stands for the electric motor's moment of inertia, which is defined as J when measured on the ICE shaft. To control the motor torque, which is limited by the

International Journal of Research in Engineering and Applied Sciences(IJREAS)
Available online at http://euroasiapub.org
Vol. 8 Issue 6, June-2018,
ISSN (O): 2249-3905, ISSN(P): 2349-6525 | Impact Factor: 7.196 |

PMSM torque limit in the field weakening area, as given in Equation (9) and which is determined as a function of angular speed, a PI controller is used.

$$T_{LIMIT} = T_{LIMIT}(\omega) \qquad (9)$$

The following diagrams depict the distinct architectural models used by the three distinct hybrid configurations (parallel, series/parallel, and series architecture), all of which share the aforementioned vehicle model.

2.2 Series/Parallel Architecture (Power-Split Device) Modelling

Figure 1 provides a mathematical description of the Power-Split Device (PSD) using the series/parallel architectural approach [15].

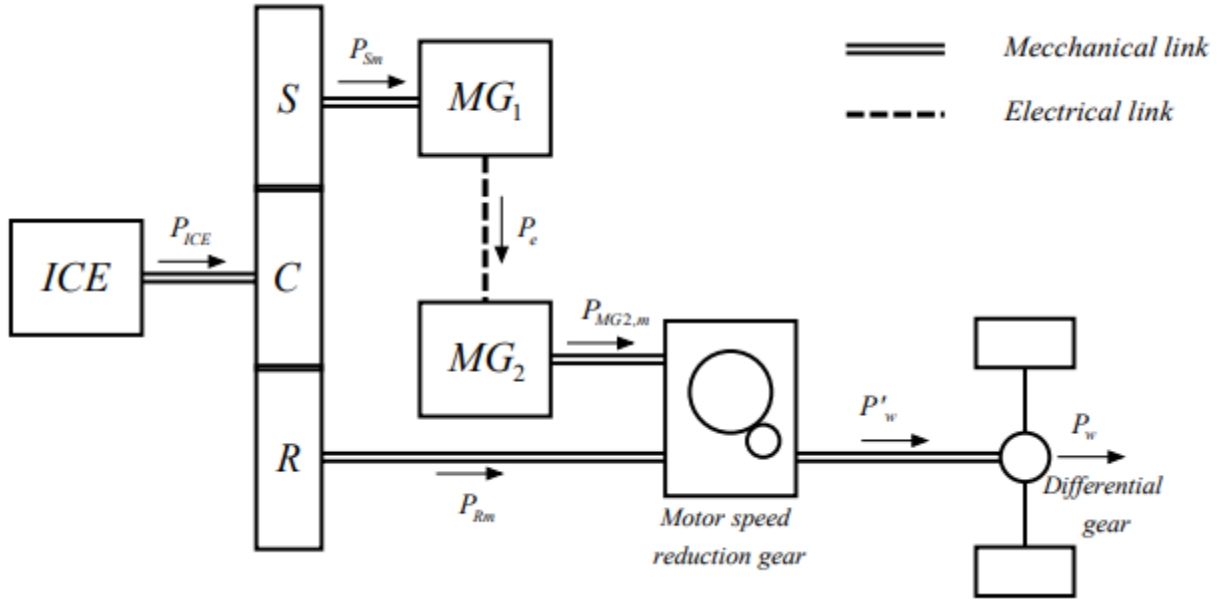

Figure 1 CVT energy convention

2.3 Series Architecture Scheme

The series architecture scheme is shown in Figure 2. Supercapacitor storage (SC) is considered in this configuration.

International Journal of Research in Engineering and Applied Sciences(IJREAS)
Available online at http://euroasiapub.org
Vol. 8 Issue 6, June-2018,
ISSN (O): 2249-3905, ISSN(P): 2349-6525 | Impact Factor: 7.196 |

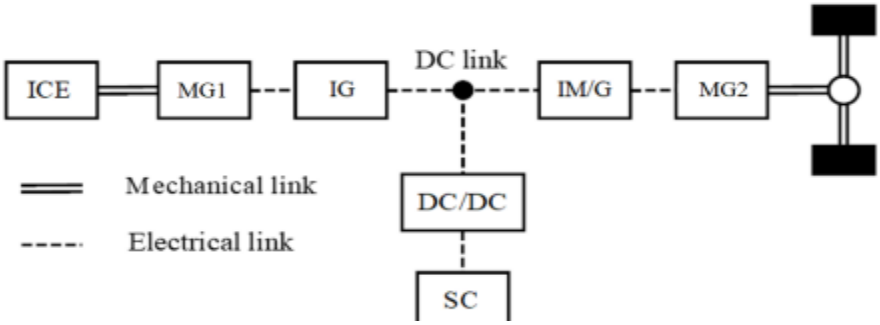

Figure 2 Series architecture scheme.

2.4 Parallel Architecture Modelling

When considering the parallel design, optimizing the powertrain is far easier than in the series/parallel situation because optimization is only needed for a single variable, ICE efficiency. Finding the optimal transmission ratio that satisfies the ICE constraints (i.e., the ICE minimum and maximum speed) while maximizing efficiency is therefore required for each working point (wheel speed, wheel torque).

It is necessary to determine the relationship between the different dynamics of the HSD's components; If the planetary rings are outwardly toothed together and fused into one, the Willis formula in Equation (10) can be used [16]:

$$\frac{\omega_R - \omega_{ICE}}{\omega_S - \omega_{ICE}} = \tau_o \qquad (10)$$

where

In Equation (10) S_z represents the sun gear and R_z represents the number of the ring- gear-tooth (conventionally negative since the teeth are internal). By combining Equation (12), Equation (13) can be derived.

$$\begin{cases} T_{ICE}\eta_m = T_S + T_R \\ P_{ICE}\eta_m = P_{Sm} + P_{Rm} \\ \left(1 - \frac{1}{\tau_o}\right)\omega_{ICE} = \omega_S - \frac{1}{\tau_o}\omega_R \end{cases} \qquad (12)$$

$$T_S = -\tau_o T_R \qquad (13)$$

From which one obtains Equation (14).

$$T_{ICE} = \frac{\left(1 - \frac{1}{\tau_o}\right)}{n} T_S \qquad (14)$$

After selecting a value for k in Equation (15), we can use that information to derive the relationship between the sun gear power and the ring gear power, as demonstrated in Equation (16).

$$\begin{cases} T_S = -\tau_o T_R \\ P_{Sm} = \omega_S T_S \\ P_{Rm} = \omega_R T_R = -\frac{\omega_R}{\tau_o} T_S \end{cases} \qquad (15)$$

$$\frac{P_{Sm}}{P_{Rm}} = -\tau_o k \qquad (16)$$

where

$$k = \frac{\omega_S}{\omega_R} \qquad (17)$$

A number of different power flow arrangements are apparent from the examination of the vehicle's energy system. Since optimizing the k-parameter is separate from the powertrain control strategy, the conditions of pure electric traction and regenerative braking are not included in the PSD optimization process.

Case 1 (MG1motor, MG2 generator): k<0, Pe<0, Psm<0, Pl1<0, PL2<0

Combining the Equations (18)

$$\begin{cases} P_e = P_{L1} + P_{Sm} \\ P_{Rm} + P_{L1} + P_e = P'_w \end{cases} \qquad (18)$$

We get Equation (19):

$$T_R \omega_R + T_S \omega_S = P'_w - P_{L1} - P_{L2} \qquad (19)$$

After some passages, Equation (20) is derived and finally one obtains Equation (21).

$$-\frac{j}{\tau_o} \omega_w T_S + kj\omega_w T_S = P'_w - P_{L1} - P_{L2} \qquad (20)$$

$$T_S = \frac{P_w / \eta_{diff} - P_{L1} - P_{L2}}{j\omega_w \left(k - \frac{1}{\tau_o}\right)} \qquad P_{L1}, P_{L2} < 0 \qquad (21)$$

International Journal of Research in Engineering and Applied Sciences(IJREAS)
Available online at http://euroasiapub.org
Vol. 8 Issue 6, June-2018,
ISSN (O): 2249-3905, ISSN(P): 2349-6525 | Impact Factor: 7.196 |

Furthermore, P'_w being defined as in Equation (22), one has Equation (23).

$$P'_w = P_w / \eta_{diff} \tag{22}$$

$$T_{MG2} = \frac{P_{L2} + P_e}{ji\omega_w} = \frac{P_{L1} + P_{L2} + P_{Sm}}{ji\omega_w} \tag{23}$$

Case 2 (MG1 generator, MG2 motor): k>0, Pe>0, Psm>0, Pl1>0, PL2>0

Combining Equations (24), and repeating the same calculations as above, one obtains Equations (25) and (26).

$$\begin{cases} P_e = P_{Sm} - P_{L1} \\ P_e - P_{L2} + P_{Rm} = P'_w \end{cases} \tag{24}$$

$$T_S = \frac{P_w / \eta_{diff} + P_{L1} + P_{L2}}{j\omega_w \left(k - \frac{1}{\tau_o} \right)} \tag{25}$$

$$T_{MG2} = \frac{P_{Sm} - P_{L1} - P_{L2}}{ji\omega_w} \tag{26}$$

Case 3 (MG1 generator–only from a mechanical point of view, MG2 generator):

k>0, Pe<0, 0<Psm<PL1, PL2>0

When the solar gear is moving at a slow enough speed to not generate enough mechanical power to compensate for the electrical losses in MG_1, this configuration often happens, and MG_2 steps in to fill the power gap. Since Equation (27) yields Equations (28) and (29), the process continues.

$$\begin{cases} P_{Sm} - P_e = P_{L1} \\ P_{Rm} + P_{L2} + P_e = P'_w \end{cases} \tag{27}$$

$$T_S = \frac{P_w / \eta_{diff} + P_{L1} - P_{L2}}{j\omega_w \left(k - \frac{1}{\tau_o} \right)} \quad P_{L1} > 0, P_{L2} < 0 \tag{28}$$

$$T_{MG2} = \frac{P_{Sm} - P_{L1} + P_{L2}}{ji\omega_w} \tag{29}$$

It is worth mentioning that the torque in each of the two motor generator configurations can be found. After determining the value of the ratio k, which is the optimization process goal shown below, the speed of the two motor generators can be obtained using the Willis formula. This allows for the computation of electrical losses and the easier acquisition of other important variables.

3. SIMULATED RESULTS

In the MATLAB/Simulink environment, three separate models were developed: a series/parallel architecture, a parallel architecture, and a series architecture. Each of these models follows a different architecture. Specifically for electric machines, power converters, and internal combustion engine (ICE) efficiency, the Simulink models incorporated the efficiency contour maps as lookup tables.

The arrows point in the direction of the positive power flows. The analysis of the gear train components does not take into account the inertial terms because of their little impact on overall efficiency. The model should be regarded as stationary since the variables in the following equations are merely algebraic, as described in Table 1.

Table 1 Variables description for simulation

Symbol	Meaning	Symbol	Meaning
MG_1	Electric machine 1	TMG_2	MG2 torque
MG_2	Electric machine 2	I	Differential gear ratio
P_e	Electrical Power	η_{diff}	Differential gear efficiency
P_{ICE}	ICE power	J	Gear ratio
PL_1	MG1 Electrical loss	η_{msrg}	Gear efficiency
PL_2	MG2 Electrical loss	ω_w	Wheel rotational speed
P_{Sm}	Sun gear mechanical power	ω_S	Sun gear speed
P_{Rm}	Ring gear mechanical power	ω_R	Ring gear speed
$P_{MG,m}$	MG2 mechanical power	ω_{ICE}	ICE speed
P'_w	Drive shaft mechanical power	τ_o	Willis constant
P_w	Wheel power	K	Sun–Ring gear ratio
T_S	Sun gear torque	T_{ICE}	ICE torque
T_R	Ring gear torque	η_m	Power split device efficiency
T_w	Wheel torque		

The objective of the PSD optimization is to find the ideal value of the transmission ratio k for each working point (for each wheel speed and wheel torque) in order to reduce fuel consumption. This optimization technique utilized a MATLAB/Simulink model to maximize the overall powertrain. Wheel speed and wheel torque are two of the many pair values that were produced in

order to get the variable k as a continuous term. The programming that was put into place allowed for the optimization of the transmission ratio function. This function essentially consists of a set of steady-state points according to the implemented model. Figure 2 shows the plotted outcome of the optimization process.

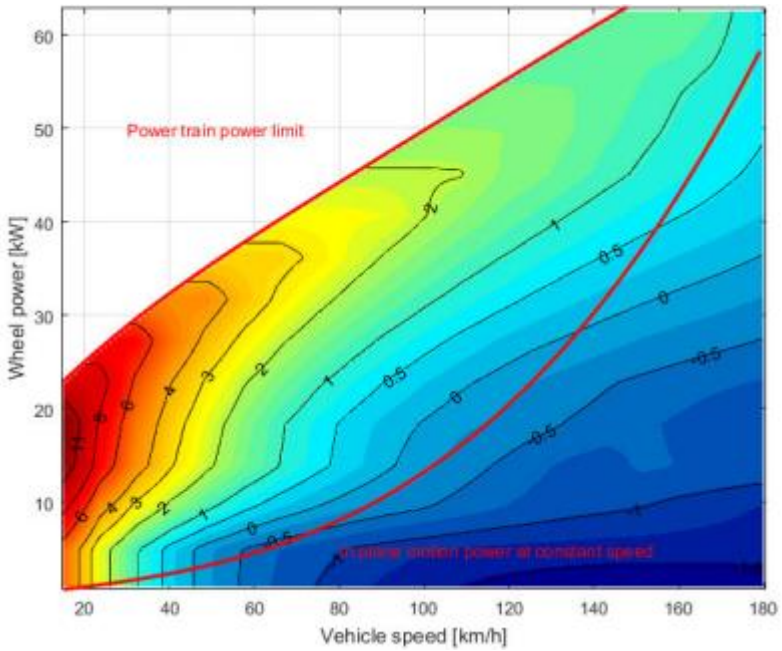

Figure 3. Steady-state function for each operating condition–CVT.

Figure 3 shows the ICE operational points that were obtained during optimization. It is clear from the optimization results that they match up with what Toyota said for ICE efficiency maximization; more especially, when comparing the optimization process to ICE losses, the electrical losses have no effect, even though they significantly affect the powertrain overall efficiency. It ought to be mentioned that this outcome was previously impossible.

International Journal of Research in Engineering and Applied Sciences(IJREAS)
Available online at http://euroasiapub.org
Vol. 8 Issue 6, June-2018,
ISSN (O): 2249-3905, ISSN(P): 2349-6525 | Impact Factor: 7.196 |

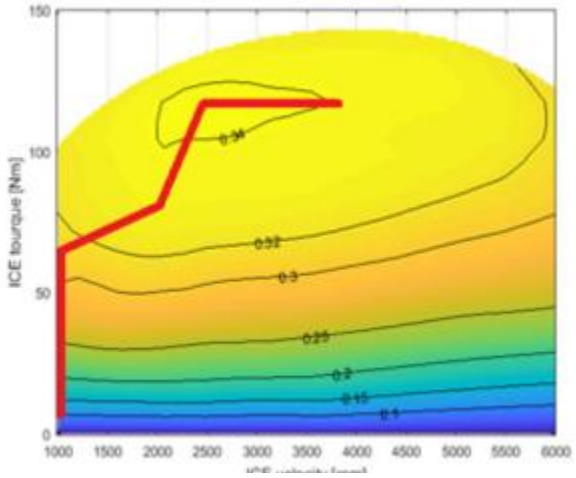

Figure 4. ICE operating points (optimal).

Figure 5 displays the optimized output for Parallel Architecture Modelling.

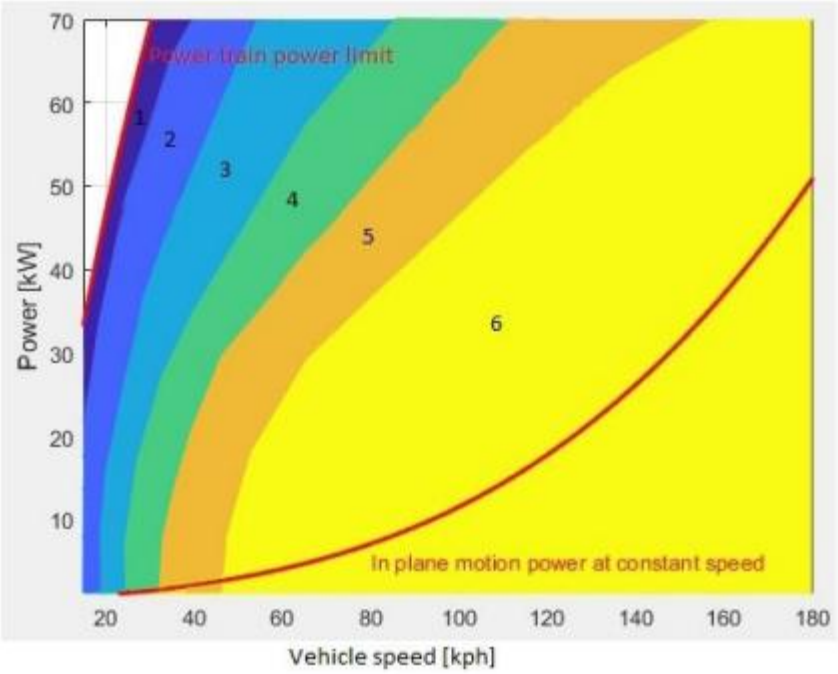

Figure 5. Optimal transmission ratio-Parallel architecture

The electric motor alone determines the vehicle's performance in a series architecture, rather than the internal combustion engine (ICE). This allows for a 50% reduction in the size of the ICE.

Vehicle Parameters based on different configurations

The three hybrid configurations that are investigated in this paper are detailed in Table 2. The electric machines, storage system, and electric converter account for approximately 80 kg, 85 kg, and 15 kg of the vehicle's mass, respectively.

Table 2 Vehicle features

Vehicle Feature	Series/Parallel	Parallel	Series
Vehicle mass (Kg)	1450	1450	1450
Rolling coefficient	0.01	0.01	0.01
Drag coefficient	0.25	0.25	0.25
Vehicle front area (m^2)	2.3	2.3	2.3
Wheel radius (m)	0.3	0.3	0.3
Differential gear ratio	3.45	10.8	8
Differential efficiency	0.97	0.97	0.97
Gear efficiency	0.95	0.95	0.95
Air density (kg/m^3)	1.22	1.22	1.22
ICE power (kW)	72	72	40
ICE maximum torque (Nm)	142	142	79
MG2 maximum torque (Nm)	163	163	230
MG2 base speed (rpm)	3000	3000	3000
MG2 maximum speed (rpm)	17,000	17,000	12,000
MG1 maximum torque (Nm)	43	-	400
MG1 base speed (rpm)	5000	-	1750
MG1 maximum speed (rpm)	1000	-	5500
DC-link voltage (V)	650	650	650

4.CONCLUSION

In recent years, there has been a growing emphasis on pollutant and greenhouse gas emissions, which has led to the increasing visibility of hybrid electric vehicles (HEVs). Despite the fact that series/parallel and parallel designs are the most frequent for medium-sized cars, this scenario

may change as a result of developments in power electronics converters and storage systems. The two energy conversions that occur in series design—namely, the generator converting ICE energy into electrical energy and the traction electric machine converting it back into mechanical energy—cause additional electrical losses. Despite the fact that series architecture makes it possible to achieve high ICE efficiency, it also results in more electrical losses. Because of this, high-efficiency storage systems and power converters have a very minor impact on parallel and series/parallel architecture, but they have a significant impact on power trains that are designed with series architecture.

REFERENCES

1. Chen, J.; Du, J.; Wu, X. Fuel economy analysis of series hybrid electric bus with idling stop strategy. In Proceedings of the 9th International Forum on Strategic Technology (IFOST), Cox's Bazar, Bangladesh, 21–23 October 2014; pp. 359–362.
2. Kim, M.; Jung, D.; Min, K. Hybrid Thermostat Strategy for Enhancing Fuel Economy of Series Hybrid Intracity Bus. IEEE Trans. Veh. Technol. 2014, 63, 3569–3579
3. Hu, X.; Murgovski, N.; Johannesson, L.M.; Egardt, B. Comparison of Three Electrochemical Energy Buffers Applied to a Hybrid Bus Powertrain With Simultaneous Optimal Sizing and Energy Management. IEEE Trans. Intell. Transp. Syst. 2014, 15, 1193–1205.
4. Uebel, S.; Murgovski, N.; Tempelhahn, C.; Baker, B. Optimal Energy Management and Velocity Control of Hybrid Electric Vehicles. IEEE Trans. Veh. Technol. 2017, 67, 327–337.
5. Yuan, Z.; Teng, L.; Fengchun, S.; Peng, H. Comparative Study of Dynamic Programming and Pontryagin's Minimum Principle on Energy Management for a Parallel Hybrid Electric Vehicle. Energies 2013, 6, 2305–2318.
6. Sierra, A.; Herrera, V.; Milo, A.; Gaztanaga, H.; Camblong, H. Experimental Validation of an Optimal Energy Management Strategy for a Hybrid Bus with Dual Storage System. In Proceedings of the IEEE Vehicle Power and Propulsion Conference (VPPC), Belfort, France, 11–14 December 2017; pp. 1–6.
7. Golchoubian, P.; Azad, N.L. Real-Time Nonlinear Model Predictive Control of a Battery–Supercapacitor Hybrid Energy Storage System in Electric Vehicles. IEEE Trans. Veh. Technol. 2017, 66, 9678–9688.

8. Jain, A.; Nueesch, T.; Naegele, C.; Lassus, P.M.; Onder, C.H. Modeling and Control of a Hybrid Electric Vehicle with an Electrically Assisted Turbocharger. IEEE Trans. Veh. Technol. 2016, 65, 4344–4358.
9. Bin Mamat, A.M.I.; Martinez-Botas, R.F.; Rajoo, S.; Romagnoli, A.; Petrovic, S. Waste heat recovery using a novel high perfor- mance low pressure turbine for electric turbocompounding in downsized gasoline engines: Experimental and computational analysis. Energy 2015, 90, 218–234.
10. Zhao, R.; Zhuge, W.; Zhang, Y.; Yang, M.; Martinez-Botas, R.; Yin, Y. Study of two-stage turbine characteristic and its influence on turbo-compound engine performance. Energy Convers. Manag. 2015, 95, 414–423.
11. Bonfiglio, A.; Lanzarotto, D.; Marchesoni, M.; Passalacqua, M.; Procopio, R.; Repetto, M. Electrical-Loss Analysis of Power-Split Hybrid Electric Vehicles. Energies 2017, 10, 2142.
12. Pellegrino, G.; Vagati, A.; Guglielmi, P.; Boazzo, B. Performance Comparison Between Surface-Mounted and Interior PM Motor Drives for Electric Vehicle Application. IEEE Trans. Ind. Electron. 2011, 59, 803–811.
13. Passalacqua, M.; Lanzarotto, D.; Repetto, M.; Marchesoni, M. Advantages of Using Supercapacitors and Silicon Carbide on Hybrid Vehicle Series Architecture. Energies 2017, 10, 920.
14. Lanzarotto, D.; Passalacqua, M.; Repetto, M. Energy comparison between different parallel hybrid vehicles architectures. Int. J. Energy Prod. Manag. 2017, 2, 370–380.
15. Adachi, S.; Hagihara, H. The Renewed 4-Cylinder Engine Series for Toyota Hybrid System; Toyota Motor Corporation: Aichi, Japan, 2012.
16. Solouk, A.; Shahbakhti, M. Energy Optimization and Fuel Economy Investigation of a Series Hybrid Electric Vehicle Integrated with Diesel/RCCI Engines. Energies 2016, 9, 1020.